 doi:10.20944/preprints202101.0137.v1

Article

Self- and Inter-Crossover Points of Jasons' Missions as New Essential Add-on of Satellite Altimetry in the Sub-Arctic Seas and the Southern Ocean

Sergei Badulin [1,2,†*], Andrey Kostianoy [1,3,†], Pavel Shabanov [1,†], Vitali Sharmar [1,†], Vika Grigorieva [1,†] and Sergey Lebedev [4,5,†]

1 Shirshov Institute of Oceanology, Russian Academy of Sciences, Nakhimovsky pr. 36, Moscow 117997, Russia; badulin.si@ocean.ru (S. B.); kostianoy@ocean.ru (A. K.); shabanov@sail.msk.ru (P. Sh.); sharmar.vd@ocean.ru (V. Sh.); vika@sail.msk.ru (V. G.)
2 Skolkovo Institute of Science and Technology, Bolshoy Boulevard 30, bld. 1, Moscow 121205, Russia
3 S. Yu. Witte Moscow University, Second Kozhukhovsky pr. 12, bld. 1, Moscow 115432, Russia;
4 Geophysical Center, Russian Academy of Sciences, Molodezhnaya St. 3, Moscow 119296, Russia; lebedev@wdcb.ru;
5 National Research University of Electronic Technology (MIET), 1, Shokin Square, Zelenograd, Moscow, 124498, Russia
* Correspondence: badulin.si@ocean.ru; Tel.: +7-499-124-75-65
† These authors contributed equally to this work.

Abstract: Satellite altimetry is successfully developing during the past three decades for the sea level, ocean dynamics, coastal oceanography, planetary waves, ocean tides, wind and wave, ice cover, Earth's gravity field, and climatology research. We propose a new essential add-on of satellite altimetry related to the peculiarities of the orbits of the Topex/Poseidon and Jasons' satellite missions which were not mentioned before in the scientific publications. Derived subsets of "self-crossover" and "inter-crossover" points in sub-polar latitudes are discussed in detail in the context of water exchange, and wind-wave dynamics, and potential challenges to be solved. The relatively short time lags between measurements at these crossovers provide additional information on anomalies of magnitudes and directions of ocean currents, and characteristics of wind-driven waves. Resulting data snapshots with constant space and time intervals can be regarded as time series of virtual buoys, an analog of continuous buoy measurements of the sea level, wind speed, and wave height. Areas of the World Ocean where these specific crossovers occur are described in the context of water exchange, wind wave studies, and potential challenges to be solved. The value of these special crossovers for studies and monitoring of the sub-polar seas is illustrated by a case study.

Keywords: Satellite altimetry, Topex/Poseidon, Jasons missions, self-crossover points, inter-crossover points, Sub-Arctic Seas, Southern Ocean, sea level, wind speed, wave height, virtual buoy

1. Introduction

Satellite altimetry is successfully developing for ocean studies during the past three decades. It shows numerous applications for the sea level, ocean dynamics, coastal oceanography, planetary waves, ocean tides, wind and wave, ice cover, Earth's gravity field, and climatology research [1–9]. The altimetry "adequate sampling ...have revolutionized oceanography" by providing data previously impossible to obtain, in the words of the outstanding oceanographer Walter Munk [10]. The TOPEX/Poseidon, "the most successful ocean experiment of all time" [10], together with its follow-on Jason's missions is operating continuously at the same reference orbits for almost thirty years. One

 doi:10.20944/preprints202101.0137.v1

should outline here the features of these orbits that generate different spatial and temporal sampling of the ocean processes [11]:

- The distance between ground tracks of these satellites varies from several kilometers in high latitudes to more than 300 km at the Equator;
- The orbit repetition period of about 10 days provides a series of cross-over points with time lag between two consecutive measurements shorter than half of this period. The locations of these points are fixed that makes them an essential component of calibration/validation procedures of the altimetry;
- The orbit inclination of 66.04° implies the coverage of the major part of the ice-free area of the World Ocean by measurements of these satellites.

The above list constitutes an idea and the essence of this study: special subsets of altimetry data with improved sampling can provide additional information on ocean dynamics and new opportunities for monitoring the seas.

In this paper we present such a subset of data of High Latitude Crossovers (HLC) with minimal time intervals between consecutive measurements and identify two of their types:

- self-crossovers (SC) when the crossover point is provided by measurements of the same satellite;
- inter-crossovers (IC) when measurements in a point are made by different altimeters, say, by a pair TOPEX/Poseidon/Jason-1, Jason-1/Jason-2 or Jason-2/Jason-3 during phases of interleaved orbits.

The crossovers, that is, points of intersection of ground tracks of altimeters play an exclusive role in maintenance of functionality and performance of satellite altimetry. Calibration and validation of measurements, assessment of the measurement corrections, retracking procedure, reconstruction of spatial and temporal fields of the measured physical quantities inevitably refer to the crossovers [3]. For the primary task of satellite altimetry, measurements of the ocean surface topography, the acceptable delay between two measurements is assumed to be less than 10 days [12]. For wind-wave studies the corresponding spatial mismatch of measurements 50 km and time delay one hour is recommended (e.g. http://globwave.ifremer.fr/products/globwave-satellite-data/satellite-crossovers). The latter implies severe limitations on the number of crossovers and orientation of the altimeter orbits. Generally, such kind of crossovers is possible to find only for different altimetry missions that dictates new difficulties to overcome. We mention only two issues among many others:

- The crossovers of different missions require their careful intercalibration accounting for features of hardware (different types of radars) and data processing methods (including different types of applied corrections);
- Incommensurability of their orbit periods excludes repetitive monitoring of the particular sites, because the corresponding crossovers appear to be unique, i.e. are irregularly distributed in space and time.

Topex/Poseidon–Jasons' missions provide special crossover datasets that are free of the above mentioned difficulties. For example, individual (for SC) and synchronized (for IC) orbits of Jason's altimeters generate regular in space and periodic in time measurements in a number of special fixed sites. The SC and IC altimeter data with regular space and time sampling can be regarded as virtual stationary sea stations, analogue of continuous buoy measurements of the sea level, wind speed and wave height. There are evident analogues in satellite altimetry of rivers when virtual water level gauges are established at locations where satellite ground tracks cross riverbed or river tributary. It makes the topic of the new crossovers quite promising, especially for the Sub-Arctic seas.

In sect. 2 we describe useful features of the CS and IC of the Topex/Poseidon–Jason's missions.

Sect. 3 describes geographical distributions of SC and IC in the World Ocean and possible gains of using the data of these special crossovers, especially, in the Sub-Arctic seas.

Sect. 4 presents a case study where advantages and problems of the data subset to be solved are discussed. The paper is finalized by Discussion and Conclusions.

Preprints (www.preprints.org) | NOT PEER-REVIEWED | Posted: 8 January 2021 doi:10.20944/preprints202101.0137.v1

2. The self- and inter-crossovers

2.1. Standard Jason's orbits. Self-crossovers

Figure 1*a* shows standard tracks of the Jason's missions in the North Atlantic. The ascending track No 165 is given in red as a reference one. The self-crossover (SC) of the orbit occurs at descending track No 168 (plus 3 to the ascending track number) near the limiting latitude $\phi_t \approx 66.05^\circ$ in a time lag a bit longer that one orbit period ($\approx$ 112 minutes). In one more orbit period (plus 5 to the reference track No 165) a similar SC occurs at lower latitude. The new crossovers with the fixed ascending track (No 165 in our case) continues to appear with every new orbit, thus, travelling to the South Pole. The passage of crossovers between poles takes approximately 1 day (about 12 orbit periods) for the fixed reference track (track No 165 in our case of Figure 1).

The part of the North Atlantic in Figure 1*a* contains 4 crossovers of this type (descending tracks are shown in green) with time intervals growing from the North to the South. Time delay of SC is growing from North to South for the fixed ascending track and from South to North for a fixed descending track. Variation of the ocean conditions between two consecutive measurements in SC, evidently, depends on time delay and on characteristic scales of variability in the particular site. Time delay is minimal in high latitudes where variability of ocean environment can be rather strong. On the other hand, low variability in tropical crossovers can essentially reduce the effect of relatively large time lag of about half-day. In this way, quality of a particular crossover is not easy to assess in advance. This important issue will be detailed in the next section.

Here one should emphasize that SCs occur regularly at the same points and time of the satellite cycle (i.e. for fixed pairs of track numbers), thus, comprising an abundant data subset. Surprisingly, this specific data set is not widely discussed and used to our knowledge.

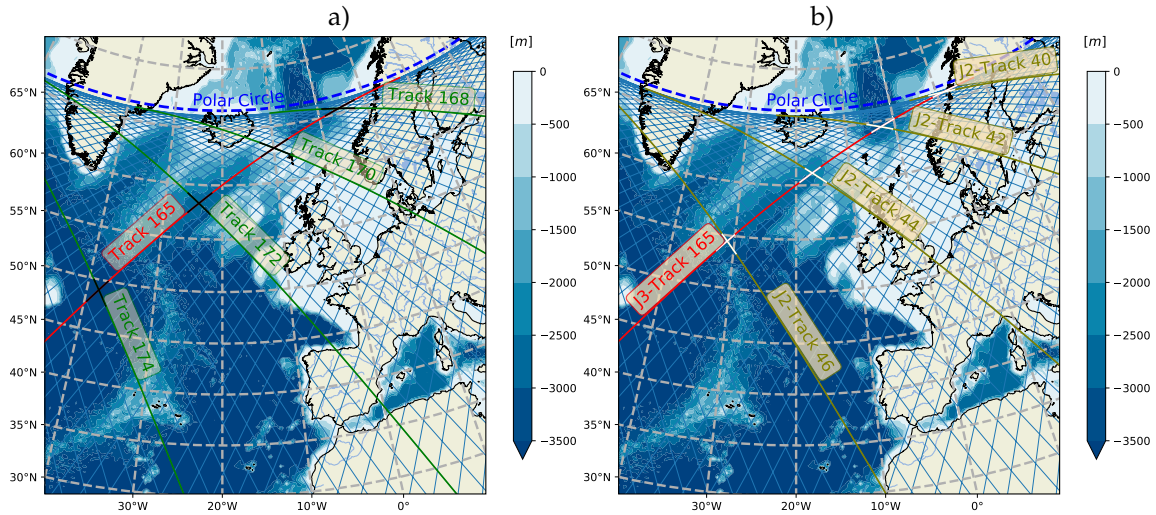

Figure 1. Crossovers of Jasons' orbits in the North Atlantic. The ascending track No 165 of Jason-3 is given in red, and green trajectories show its descending counterparts generating crossovers within the one-day delay. a) – self-crossovers (SCs) of Jason-3 standard orbits; b) – inter-crossovers (ICs) of Jason-3 and Jason-2 during the phase of interleaved orbits October 2016–April 2017.

2.2. The Jason's interleaved orbits. Inter-crossovers

At the beginning of every new mission (Topex/Poseidon – Jason-1; Jason-1 – Jason-2; Jason-2 – Jason-3) two satellites conform a special configuration of the so-called interleaved orbits when "old" satellite is positioned midway between standard ground tracks and two satellites are placed on opposite sides of the Earth. These phases have been realized in mid-September 2002–October 2005 for the tandem TOPEX/Poseidon–Jason-1, mid-February 2009–March 2012 for Jason-1/2, mid October 2016–April 2017 for Jason-2/3. The new configuration of two orbits provide a new family of crossovers

Preprints (www.preprints.org) | NOT PEER-REVIEWED | Posted: 8 January 2021 doi:10.20944/preprints202101.0137.v1

we call inter-crossovers (IC). For IC the shortest time lag between consecutive measurements is about one-half of the orbit period (56 minutes). It occurs near the latitudes approximately 65.95° in the Northern and Southern Hemispheres, i.e. a bit closer to the limiting latitudes of the orbits than SCs. As a result, similar ICs with longer time delay (approximately $1\frac{1}{2}$, $2\frac{1}{2}$ ... orbit periods) conform a configuration resembling the SC one as shown in Figure 1*b* for the same reference track of Jason-3 No 165 and descending tracks of Jason-2 No 40, 42, 44, and 46.

Table 1 presents latitudinal dependencies of variability of parameters measured by altimeter for the ICs with the fixed ascending track No 165 of Jason-3 and Jason-2 tracks No $40-52$. The estimates are given for all the duration of the phase of interleaved orbits (October 2016–April 2017, totally, 19 cycles). Similar estimates can be made for SCs in Figure 1*a*.

The northest IC has a minimal time lag a bit more than 1 hour, the southest one No 52 in Table 1 – more than half-day (13 hours 40 min.). Variability of significant wave height H_s and normalized radar cross-section σ_0 directly measured by altimeters grows in moderate latitudes with the time lag. The standard deviation (STD) of difference of measurements of Jason-2 and Jason-3 in IC with time lag about 9 hours (Jason-2 track 48, line 5) is 6 times higher than one of minimal time lag for wave height H_s (column 5) and more than 3 times for normalized radar cross-section σ_0 (column 7). The variability is even stronger for extreme values (columns 6 and 8) exceeding one order of magnitude for H_s. The variability weakens in tropical and subtropical ICs (lines 6, 7) but still remains higher than in the Sub-Arctic IC with the minimal time delay.

Table 1. Variability of the altimetry measurements of ICs during the phase of interleaved orbits of Jason-2/3 (mid October 2016 – April 2017). Track No 165 of Jason-3 is taken as a reference one, track numbers of Jason-2 are shown in the first column.

Jason-2 track number	Latitude deg.	Longitude deg.	Time lag sec	STD(ΔH_s) meters	MAX(ΔH_s) meters	STD($\Delta\sigma_0$) dB	MAX($\Delta\sigma_0$) dB
40	65.94	10.56	3708	0.223	0.367	0.265	0.871
42	64.39	-3.59	10693	0.453	1.050	0.345	1.260
44	60.87	-17.68	17725	0.527	1.304	0.617	2.393
46	54.00	-31.88	24868	1.028	3.662	0.878	3.246
48	40.25	-46.06	32261	1.311	4.345	0.825	3.250
50	11.73	-60.23	40207	0.202	0.424	0.509	1.382
52	-25.40	-74.41	48476	0.359	0.744	1.987	2.137

An additional aspect of this variability is its effect on numerous corrections of altimetry measurements. Some of these corrections are directly linked with the time delay, e.g. tidal corrections. Other corrections, like Sea State Bias (SSB), are estimated parametrically [13–15] as functions of the directly measured values (e.g. H_s and σ_0). One can easily show that all these corrections are minimal for the HLCs with minimal time lags that nudges us to draw special attention to these crossovers located near the Polar Circles. These special crossovers provide an additional information on anomalies of ocean currents, and characteristics of wind-driven waves and near-surface winds [altimetric wind speed, e.g. 16]. The angle between the tracks in the SCs and ICs is quite large (about 30° and 15° correspondingly) that can be used for calculation of quasi-instantaneous values of:

- anomalies of geostrophic current velocities and their directions [17–19];
- wave heights, periods and directions of wind-drives seas [15,20,21].

It should be stressed that an instantaneous assessment of the geostrophic currents governed by balance of the Coriolis force and the sea surface height anomaly (SSHA) gradient is, generally, unattainable in the classic altimetry. Usually, estimates of non-collinear components of the geostrophic velocity vector are widely spaced over time. Interpolation of altimetry data in space and time is used to construct a generalized field of the ocean circulation. It leads to undersampling of relatively fast and small-scale ocean dynamics, especially, in the Sub-Polar seas where the Rossby radius of deformation is small.

Preprints (www.preprints.org) | NOT PEER-REVIEWED | Posted: 8 January 2021 doi:10.20944/preprints202101.0137.v1

The instantaneous along-track assessment of geostrophic currents with SCs and ICs near the limiting latitudes becomes a worthy solution of the problem.

2.3. Crossover clusters. Temporal sampling of SCs and ICs

As menioned above, inter-mission crossovers are irregularly distributed in space and time due to different periods of satellites. The standard orbits of the T/P and Jasons' missions gives an essential advantage providing fixed periodically spaced sites where crossovers occur each cycle of approximately 10 days. Different types of these crossovers can be grouped into clusters as shown in Figure 2 for the phase of interleaved orbits of Jason-2/3 (October 2016 – April 2017). Further on, we refer to this phase if otherwise stated.

Table 2. Spacing of crossovers with minimal time lag

Type of crossover	Latitude	Longitude to IC 23, 32	Time lag sec	Track number 1 to Jason-3 of IC 32	Track number 2 to Jason-3 of IC 32
IC 32	65.94	0	3707	0	-125
IC 23	66.00	0	3261	+129	0
SC 22	65.44	+0.71	6973	+228	+231
SC 33	65.44	-0.71	6973	+152	+155

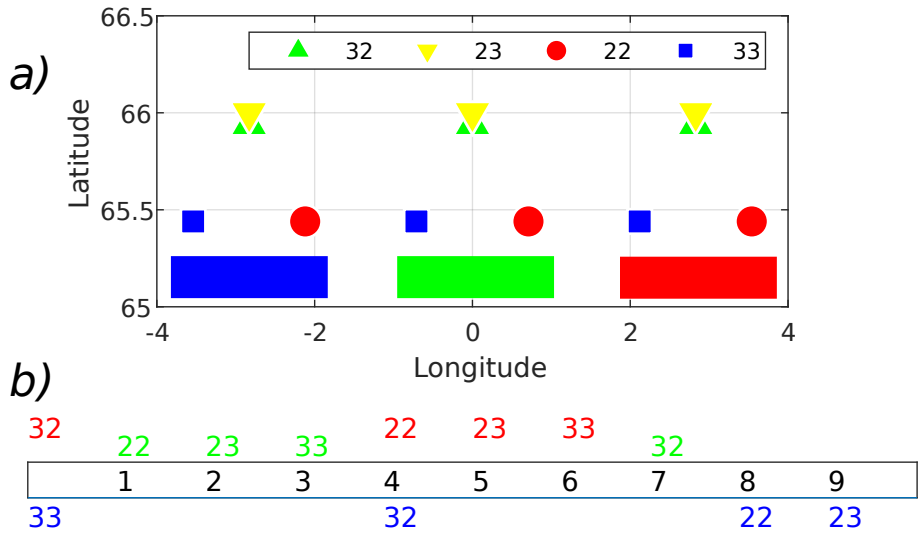

Figure 2. Crossover clusters with minimal time lags. a) – Relative location of three clusters. Symbols and codes of SCs and ICs are given in legend; b) – Timeline of crossovers in days of cycle (black number $1-9$) relatively to IC 32 of the central cluster, code color correspond to the cluster colors in panel *a*.

We introduce codes for particular crossovers: "22" and "33" mean SCs of Jason-2 and Jason-3 correspondingly. The "IC 23" means that Jason-2 passes the crossover before Jason-3 and "IC 32" is used for an opposite case. Each cluster comprises 2 SCs (red circlres and blue squares) and 2 ICs (green and yellow triangles) centered relative to the ICs latitude. Table 2 presents key characteristics of the cluster of crossovers with minimal time lags we are mostly interested in. The cluster's SCs are located at approximately the same latitude about 65.44° N(S). IC 32 is approximately 30 nautical miles to the North (South) close to the latitude 65.94° and its counterpart IC 23 is 3.6 nmi more apart to the North (South) at the same longitude. Time delays for SC 22, 33 are evidently very close to each other because of equivalence of individual orbit periods of satellites (column 4 of Table 2). Difference about 9 minutes of time lags of ICs is explained by shift of Jason-2 and 3 orbits slightly different than one-half of the orbit period. Taking the track number of Jason-3 of IC 32 as a reference one can get the track numbers of all elements of the cluster following rules of two last columns of Table 2 (track number more than 254 means a shift on one cycle).

Preprints (www.preprints.org) | NOT PEER-REVIEWED | Posted: 8 January 2021 doi:10.20944/preprints202101.0137.v1

Figure 2 shows location of three clusters (panel *a)*) together with timeline of crossovers in Figure 2*b*. Codes of crossovers correspond to colors of the clusters. One can see that the group of three clusters provide at least 1 measurement per day for distance of approximately 212 nmi along latitude. As shown below many crossovers with minimal time lag are located in ocean straits. Thus, the issue of clustering of SCs and ICs can be useful for assessment water mass transport accross these areas.

All the said above predetermines our special attention to the high latitude SCs and ICs with minimal time lags, their geographical distribution, and features of dynamics.

3. Geography of high latitude crossovers: issues of monitoring Sub-Polar seas

In this Section we discuss the geographic location of SC and IC points with minimal time lags in both hemispheres, which fortunately cross a series of very important for oceanography water bodies (Figure 3):

1. The Norwegian Sea;
2. The Denmark Strait;
3. The Davis Strait;
4. Foxe Basin north of Hudson Bay in the Canadian Arctic Archipelago;
5. The White Sea;
6. The Bering Strait;
7. The Southern Ocean.

Sea ice conditions in the White Sea, Foxe Basin, the Bering Strait, and along Antarctica can significantly affect quantity and quality of the altimetry data. Below we show all these areas in their connection with specific tasks for their studies and monitoring.

3.1. The Norwegian Sea

In the Norwegian Sea, the chain of 18 SCs and 18 ICs forms 9 full clusters in the southern part of the sea between Iceland and Norway (Figure 3*a*). This cross-section is one of the key sections in the World Ocean because it determines water exchange between the North Atlantic Ocean and the North Sea with the Norwegian Sea. This is an important area where calculations of water mass and heat transfer from the Atlantic Ocean to the Arctic Ocean are made to understand climate change in the Arctic Ocean. Large-scale ocean circulation in the Norwegian Sea and adjacent areas largely determines the climate in the North Atlantic Ocean [22–28].

The hydrological regime of the Norwegian Sea is determined by the flux of the Atlantic water, transferred by the Norwegian Current (a branch of the North Atlantic Current) through the Faeroe–Shetland Strait. Also a small part of the Atlantic water penetrates between Iceland and the Shetland Islands. Besides, freshened water of the Baltic Current comes from the North Sea along the coast of Norway. The total volume of the Atlantic water coming to the Norwegian Sea amounts to about $100,000$ km^3/year, and water carried out to the Atlantic Ocean – about $40,000$ km^3/year. The maximum inflow of water in the Norwegian Sea is observed in December and January, the minimum in April and May. The magnitude of interannual fluctuations of the Atlantic water inflow reaches $40,000$ km^3/year [29,30]. The chain of new crossovers crosses the following currents which determines water exchange between the North Atlantic Ocean and the Norwegian Sea (from west to east): *(i)* the Coastal Iceland branch of the Irminger Current; *(ii)* the East Icelandic Current which flow southward around eastern coast of Iceland; *(iii)* the Norwegian Current, and *(iv)* the Norwegian Coastal Current (to the south of 65°N it is called the Baltic Current) which flow northward into the Norwegian Sea [29,30].

A possibility of along-track estimates of geostrophic current magnitudes and directions at the high latitude SCs and ICs from instantaneous SSHA provided by altimetry represents a strong advantage in establishing permanent monitoring of fields of currents and calculation of precise water exchange anomalies between sub-basins in this region. 9 clusters provide at least 3 independent estimates of the current field across the cross-section per day (see sect. 2.3 and Figure 2). Thus, currents and water

 doi:10.20944/preprints202101.0137.v1

exchange can be monitored with essentially better time resolution that is usually made on the basis of gridded altimetry products for SSHA.

The region is also characterized by intense wind wave variability, especially in the conditions of severe weather which is a characteristic feature of the region. In winter season, wave heights can exceed 20 m, while the duration of "weather windows" (periods with waves less than 1.5 m) is never more than 3 days [31]. Wave models reproduce the wave and wind fields in the Norwegian Sea with high accuracy, showing a good correlation with buoy measurements [32,33]. Nevertheless, permanent wave monitoring at the HLCs can further support the analysis of the sea state under ongoing climate change. Being concentrated near the Polar Circle away from stationary buoys, these points can be also used for the additional calibration and validation of wave models.

3.2. The Denmark Strait

In the Denmark Strait, the chain of 4 full clusters (8 SCs and 8 ICs) and 5 more SCs in the near-shore zone is located between Greenland and Iceland, just southward of the southern border of the Greenland Sea (Figure 3*b*).

The strait stretches 480 km long and 290 km wide, and has a sill of 191 m depth at the Greenland-Iceland Rise. Being relatively narrow it plays an exceptional role in the ocean circulation and water transport in the North Atlantic Ocean. In the Denmark Strait, the East Greenland Current flowing southward meets the northern branch of the Irminger Current (also known as the North Icelandic Irminger Current) flowing around Iceland northward, and forms the East Greenland Frontal Zone [29,30]. That is why most of hydrographic surveys, theoretical and model studies in this region are focused on the water transport between the Greenland Sea (Iceland Sea) and the North Atlantic Ocean [34–36]. Repeated transects across the Denmark Strait based on local SCs and ICs allows one to derive new high accuracy time series of sea level, current velocity, water transport, significant wave height (SWH), and wind speed measurements, and to compare them with standard oceanographic (CTD, ADCP) and wave data (visual observations, model simulations, and buoy measurements).

The Greenland ice sheet essentially conditions the features of storm activity in this area, in particular, the phenomena of bora-types in the western part of the section called a "Piteraq". This is a very strong katabatic wind which rush down the east coast of Greenland usually in the autumn and winter. Wind speeds typically reach $50-80$ m/s ($180-288$ km/h). On 6 February 1970, the Tasiilaq village located southward of the Denmark Strait was hit by the worst Piteraq ever documented in Greenland with estimated wind speed of 90 m/s (325 km/h) causing severe damage. Since the beginning of 1970 special Piteraq warnings are issued by the Danish Meteorological Institute [37]. Measurements of wind speed at the HLCs in the Denmark Strait can contribute to the understanding the characteristics and impact of the Piteraq on water area and estimate the distance of its impact from the coast.

3.3. The Davis Strait

The chain of 3 full clusters (6 CSs and 6 ICs) and 3 more nearshore SCs is located in the narrowest part of the Davis Strait, between the Baffin Island and western coast of Greenland, right in the middle of the strait which stretches from 70° to 60°N where it meets the Labrador Sea (Figure 3*c*). The width of the strait is between 300 and 1000 km, and its depth varies from 350 to 500 m at the sill in the narrowest part along the Arctic Circle. The Davis Strait separates the Baffin Bay and the Labrador Sea. This area is poorly understood due to a lack of in-situ measurements.

Preprints (www.preprints.org) | NOT PEER-REVIEWED | Posted: 8 January 2021 doi:10.20944/preprints202101.0137.v1

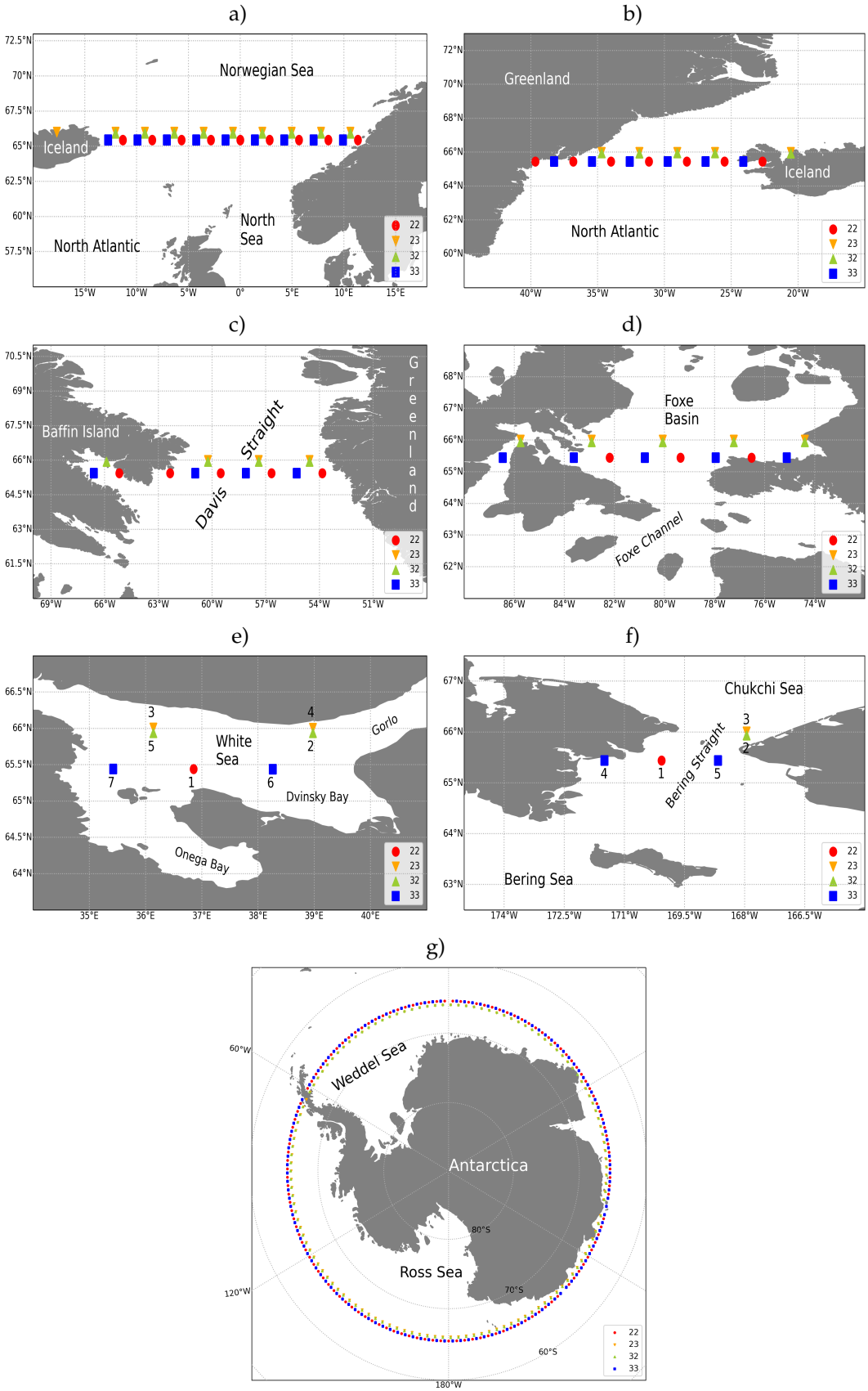

Figure 3. SCs and ICs of the phase of interleaved orbits of Jason-2/3: a) – the Norwegian Sea; b) – the Denmark Strait; c) – The Davis Strait; d) – the Foxe Basin; e) – the White Sea; f) – the Bering Strait; g) – the Southern Ocean.

Preprints (www.preprints.org) | NOT PEER-REVIEWED | Posted: 8 January 2021 doi:10.20944/preprints202101.0137.v1

Two currents pass through the strait in different directions. The relatively warm West Greenland Current carries water along the coast of the West Greenland to the north, and the cold Labrador Current – along the eastern coast of the Baffin Land to the south, into the Labrador Sea and further into the Atlantic Ocean. The cold current carries numerous icebergs breaking away from the Greenland Ice Sheet in Melville Bay. Thus, near the eastern coast of the strait, the conditions for navigation are noticeably better, the navigation season in this part of the strait lasts from mid-summer to late autumn, and it was there that fishing and whaling vessels traditionally went north. At this time of the year, the main ports of Greenland are in operation: Paamiut, Nuuk and Sisimiut. In the winter months, more than 50% of the water area is covered with ice, while in the warm season, more than 90% of the water area is ice-free [38]. More than 90% of the water area of the Davis Strait is used for navigation: from 50 to 70 large-tonnage vessels are constantly in the waters of the strait, and the total number of vessels passing through the strait ranges in different years from 400 to 700. The main types of vessels are fishing, cargo and passenger, including coastal ferries off the Greenland coast, tourist liners, and tankers [38,39].

Regular satellite altimetry tracks crossing the Davis Strait allow assessing anomalies of water exchange between the Baffin Bay and the Labrador Sea. During the ice-free period there is a possibility to establish a permanent monitoring of water exchange through the Davis Strait, and of the West Greenland and Labrador currents. These measurements can contribute significantly to the oceanography of this region under climate change.

The non-Jasons' tracks are almost parallel to the strait axis and, thus, their use for instantaneous assessment of water mass transfer accross the strait is questionable. On the contrary the Jasons' satellite tracks are close to zonal directions, i.e. they better capture geostrophic currents along the strait axis. The instantaneous currents can be successfully estimated from two intersecting tracks with a short time lag. A similar approach was tested in the Caspian Sea when calculating water exchange between sub-basins from satellite altimetry data [18,19]. Jasons' HLCs with minimal time lags make such periodic in time along-track estimates at fixed sites more adequate to the problem of monitoring water exchange.

The Arctic warming shows new opportunities for intensification of shipping via the Northwest Passage which starts from the Davis Strait [39]. The present and future shipping activities (including those related to offshore oil and gas exploration) require better knowledge on wind and wave regime in this area which can be gained from the advantages of satellite altimetry including those related to measurements of wave characteristics at SCs and ICs.

3.4. Foxe Basin

The length of the Foxe Basin in the Canadian Arctic Archipelago is of 600 km and width of 500 km. The chain of 4 full clusters (8 SCs, 8 ICs) and 2 ICs in the main water body, and one SC in the eastern nearshore area covers the basin between the Melville Peninsula on the west and the Baffin Island on the east (Figure 3*d*), the Frosen Strait and the Roes Welcome Sound. The basin is shallow with depths of 100 m in the northern and central parts, and up to 400 m in the southern part which is connected with the Hudson Bay on the west and Hudson Strait on the east via Foxe Channel. Foxe Basin is rarely ice-free even in summer season which complicates all types of oceanographic observations. Tidal currents and strong winds keep the ice pack in constant motion and contribute to the formation of numerous polynyas and shore leads which are found throughout the region, especially in the southern part of the Foxe Basin. Regional warming allows establishing monitoring of wind-wave characteristics and water exchange between Foxe Basin and Hudson Bay during $2-3$ months with the help of satellite altimetry, and to contribute significantly in the unknown oceanography of this area with a unique wildlife.

3.5. The White Sea

In the White Sea, two incomplete clusters (3 SCs and 4 ICs) are located in the middle of the sea (Figure 3*e*). The crossover events occur 7 different days of each 10-day Jason's cycle, thus, providing

Preprints (www.preprints.org) | NOT PEER-REVIEWED | Posted: 8 January 2021 doi:10.20944/preprints202101.0137.v1

a reasonably good temporal coverage of the area. The White Sea has a very complicated shoreline, complex water dynamics conditioned by wind forcing, water exchange with the Barents Sea in its northeastern part, strong tidal motions and river inflows [30,40–43]. The cyclonic activity over the White Sea is quite intense forming specific wind-wave climate. In winter, wind-wave regime is determined mostly by the influence of the Icelandic Low, in summer season, it is formed under the influence of Arctic invasions of cold air. The storminess activity in the White Sea is relatively low due to its small size (about 250 × 250 km) and winter ice cover.

In general, the White Sea is well studied region covered by visual observations, stationary buoys and weather stations measurements complemented by numerous national research programs, sea expeditions [41], global and regional wind-wave models [44]. Nevertheless, 3 SCs and 4 ICs in the White Sea can be used as an alternative source of valuable data on sea level variability, tides, currents, water exchange with the Barents Sea, wind and wave regime, and ice cover [45,46]. Satellite altimetry is already applied to the White Sea in order to study sea level variability, tidal, wind and ice regime [17,18,47–51].

3.6. The Bering Strait

In the Pacific Ocean, 3 SCs and 2 ICs fall exactly into the Bering Strait (Figure 3*f*), which is of great value for the assessment of water exchange between the Pacific and Arctic oceans. The Bering Strait 90 km wide and 60 m deep has a cross-section of 3.4 km^2. The water transport mainly directed into the Arctic Ocean varies between 0.5 to 2.5 Sv in relation to atmospheric condition (local winds and atmospheric pressure). The strait is usually completely frozen over from October to June [30,52]. Probably the first extensive survey of the Northern Bering Sea was carried on in mid 1980s for 5 years in the scope of the NSF ISHTAR Program [30,53]. The observations were concentrated in the summer months with the objective of determining the main physical, chemical and biological characteristics of the Northern Bering Sea in typical summer situations. The ISHTAR Program included, beside extensive field surveys, the application of a three-dimensional General Circulation Model derived and adapted to the Northern Bering Sea from the three-dimensional model developed at the GeoHydrodynamics and Environmental Research Laboratory (GHER) of the University of Liege, Belgium [30,54–57]. The objectives of the model were to gain a general understanding of the Northern Bering Sea dynamics in the summer season, including modelling of the currents in the Bering Strait which were compared with measurements at buoys deployed in summer 1985 and 1986.

Now, a regular monitoring of water exchange can be based on the evaluation of the vectors of geostrophic velocity for every Jason cycle (i.e. about 10 days) at 5 crossovers (Figure 3*f*). This will provide unique regular information on water exchange between the Bering Sea and Chukchi Sea with a step of 10 days for the past 30 years since the beginning of the Topex/Poseidon mission in September 1992. Wind and wave measurements are also of high value taking in mind intensification of shipping activities along the Northern Sea Route with a decline of the Arctic sea ice cover.

3.7. The Southern Ocean

In the Southern Hemisphere, crossovers form a belt ranged between 65.5° and 66.0°S near the Antarctic Circle (Figure 3*g*). The points do not cross the Polar Front (PF) and the Antarctic Circumpolar Current (ACC), but in some places they cross the Southern Boundary (SB) of the ACC and the Antarctic Slope Front (ASF) located over the upper continental slope of Antarctica (for example, close to the Drake Passage from the side of the Pacific Ocean) [30,58–62]. In the ice-free conditions it would be possible to measure ocean currents, eddies, calculate energy of jets and eddies. Regular measurements of wave heights and periods can fill the gaps in the sea state data in the Southern Ocean caused by a lack of buoys and visual observations, and can also be used to validate wave models. The experiment is complicated by ice conditions, but the regular coverage of the area with crossover points (497 by about 16,000 km) will doubtless be useful for better understanding of the ongoing metocean processes in the coastal zone of Antarctica.

Preprints (www.preprints.org) | NOT PEER-REVIEWED | Posted: 8 January 2021 doi:10.20944/preprints202101.0137.v1

4. High latitude crossovers in the Norwegian Sea

4.1. High latitude crossovers for assessment currents and wind sea state

Assessment of large-scale current velocities is a key output of the satellite altimetry for ocean studies. Assuming a balance of the Coriolis force and pressure gradient due to deviation of sea surface from equipotential surface of the Earth gravity field one has

$$2\Omega \mathbf{U}\mathbf{n} \sin\phi = -g\nabla\eta\mathbf{s} \tag{1}$$

where $2\Omega = f$ is the Coriolis parameter and ϕ is the latitude of the site of measurements, $\mathbf{s}$ is the along-gradient orth vector and $\mathbf{n}$ is normal orth to $\mathbf{s}$. Velocity vector $\mathbf{U}$ in equation (1) is always orthogonal to the pressure gradient. Figure 4*a* provides the well-known scheme of altimetry measurements of currents in a crossover point. Non-parallel tracks (red – ascending like in our previous figures, green – descending) allow for estimating components of the geostrophic current which are perpendicular to the track directions (red and green dashed lines). The linearity of (1) eases estimates both of the values and their errors. One should stress that the scheme does not lead to ambiguity of the current directions because of the important feature of linearity.

Anomalies of current velocity can be used for calculation of anomalies of water transport, or can be transformed into absolute current velocity by adding the Mean Dynamic Topography derived from the difference between the mean sea surface and the geoid, or from ocean drifters and hydrographic profiles.

The physical model of wave periods from altimetry data [20] is also based on estimates of spatial gradients and, in this sense, is an analogue of the above scheme. The result of the model can be expressed in a quite compact relationship between wave steepness and the spatial gradient [20,21]

$$\mu = \frac{\alpha_{ss}^{3/5}}{2^{2/5}} |\nabla H_s|^{1/5} \approx 0.596 |\nabla H_s|^{1/5} \tag{2}$$

where $\alpha_{ss} \approx 0.67$ is dimensionless parameter of the theory of weak turbulence of wind-driven waves [63,64] the equation (2) is based on. Wave steepness is defined in terms of significant wave height H_s and spectral peak period T_p

$$\mu = \frac{\pi^2 H_s}{g T_p^2}. \tag{3}$$

The appearance of gradient of H_s in the basic relationship (2) is associated with two important features of the physical model [20]. First, the fetch-limited scenario of wind-wave evolution is considered as the most adequate to the dynamics of wind-driven sea [65–67]. It allows to relate variations of wave height with spectral flux of energy which is documented by instantaneous sea state parameters: wave height and wave period. Secondly, the model implies that these variations of H_s (∇H_s) are aligned with the direction of wave group velocity (general direction of wave propagation). In this way, the model "forgets" the wave direction and operates with the gradient projection. Thus, an ambiguity of wave direction of the type "back-forth" in this scheme of altimetry measurements appears. Figure 4*b* shows gradients of H_s for estimates of wave steepness and, then, wave period in the spirit of the similar scheme for geostrophic currents in Figure 4*a*.

Figure 4 also shows a possible problem of HLCs when angle between tracks is rather small. Errors of measurements can affect significantly estimates of directions. In the case of wind wave measurements high nonlinearity of the relationship (2) mitigate the problem when angle between track and wave direction is not too close to $\pi/2$. Generally, the single track measurements give rather good approximation [21]. On the contrary, linearity of the geostrophic relationship (1) becomes a problem when estimating currents at low angles α in Figure 4*a*.

Preprints (www.preprints.org) | NOT PEER-REVIEWED | Posted: 8 January 2021 doi:10.20944/preprints202101.0137.v1

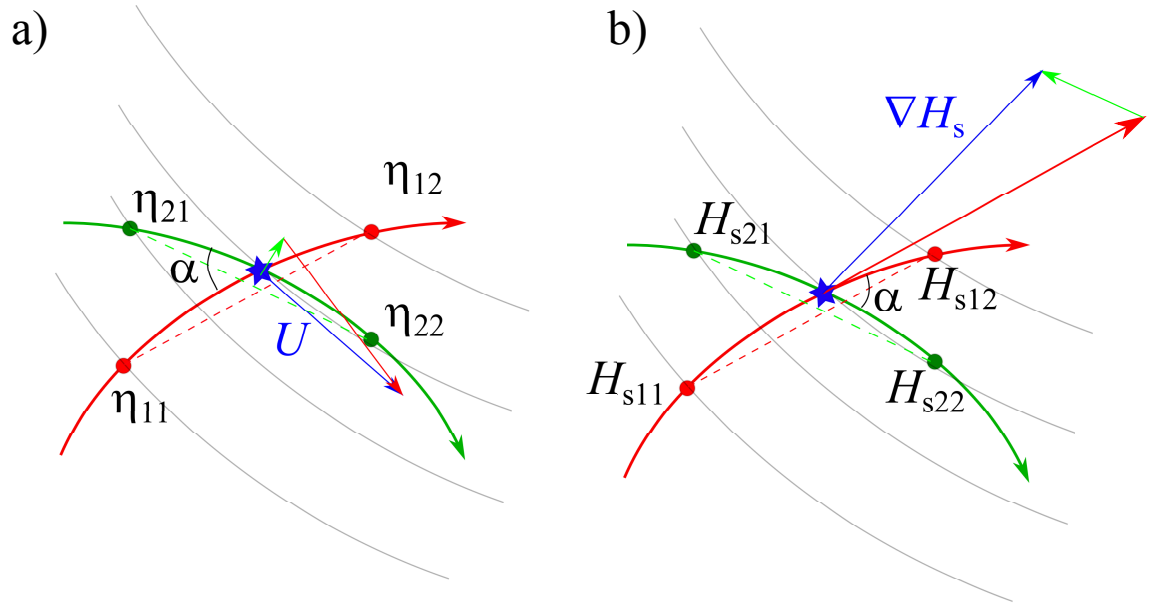

Figure 4. Setups of altimetry measurements in a crossover point. *a* – measurements of large-scale currents by satellite altimeter. Along-track differences of the sea surface height anomaly $\eta_{12} - \eta_{11}$ and $\eta_{22} - \eta_{21}$ are used to get transversal projection of the current velocity; *b* – measurements of wave steepness. Along-track differences of the significant wave height H_s $(H_{s12} - H_{s11})$ and $(H_{s22} - H_{s21})$ are used to estimate along-track components of ∇H_s

In below sections we discuss features of reconstruction of slowly varying large-scale currents and sea waves as it is documented by reanalysis of the Copernicus Marine Service (https://marine.copernicus.eu/) and reconstructed from along-track estimates of the HLC. The Norwegian Sea is a good area for such a study. HLCs form a regular array of 9 full clusters and, thus, provide at least 3 daily measurements in the crossover points.

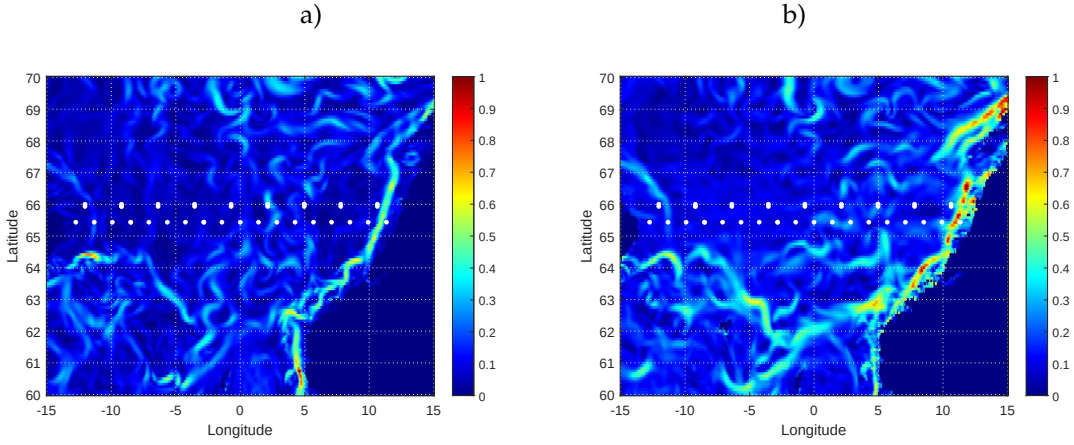

Figure 5. Geostrophic currents in the Norwegian Sea from the GLORYS12V1 reanalysis. Current velocity modula in m/s for 17 (a) and 27 (b) October.

4.2. Geostrophic currents in the area between Iceland and Norway

The GLORYS12V1 product has been used for assessment of large-scale currents. The data is provided at a standard regular grid at $1/12^\circ$ (approximatively 8 km) resolution. This eddy resolving reanalysis is based on altimetry data since 1993. We choose the period 17 October 2016 – 27 October 2016 covering the whole cycle of Jasons' altimeters. The componens of surface current velocity for the date 17,October are presented in Figures 5a,b. The absolute values of the current velocity are shown in

Preprints (www.preprints.org) | NOT PEER-REVIEWED | Posted: 8 January 2021 doi:10.20944/preprints202101.0137.v1

Figures 5c,d for the first and the last (27 October) days of the period under study. The figures reflect the complicated structure of jets in this area described in sect. 3.1. At the same time, the fine structure of the currents that visually correlates with directions and locations of Jasons' tracks look somewhat suspicious. This distrust is confirmed by trivial spectral analysis.

Figures 6,7 present two cross-sections along latitudes $\phi = 66^\circ$ and $\phi = 66.5^\circ$, i.e. only 30 nmi to the North. The zonal component U and the meridional one V demonstrate general feature of circulation in the area shown in Figure 5. The meridional component of the current V is directed to the North along the main eastern part of the transect between Iceland and Norway in full agreement with distribution of the Coastal Iceland branch of the Irminger Current and the East Icelandic Current which flow southward around eastern coast of Iceland (see western side of the transect) and the Norwegian Current and the Norwegian Coastal Current which flow northward into the Norwegian Sea. Several peaks directed northward represent known branches of the Norwegian Current and the Norwegian Coastal Current at coast of Norway.

Fourier decomposition of function $G(\lambda)$ (λ is longitude and G is a current velocity component)

$$G(\lambda_k) = \sum_n^N A_n \exp\left(-\mathrm{i}2\pi\Lambda_k\right) \tag{4}$$

where the spatial frequency

$$\Lambda_k = \frac{(n-1)(\lambda_k - \lambda_W)}{\lambda_E - \lambda_W} \tag{5}$$

discovers pronounced periodicity of the transects (λ_W, λ_E are Western and Eastern boundaries of the transect). Figures 6,7*c,d* show spectral densities of the current components $S_n(\Lambda) = A_n^2$ as function of the spatial period $1/\Lambda$. For the latitude $\phi = 66^\circ$ slightly below the limiting for the Jasons' missions (Figure 6*c,d*) the spectral peaks at the period $\approx 1.42^\circ$ matches the spacing of Jason's 254 tracks ($360^\circ/254 \approx 1.4173^\circ$). Only 30 nmi ($\approx 55.56$ km) to the North the period of spectral peak becomes 50% longer ($\approx 2^\circ$). This example clearly shows possible problems of the reanalysis based on the altimetry data near the latitude where an essential fraction of data (Jasons' data) disappears.

The problem of the current reanalysis is confirmed by comparison with along-track estimates of geostrophic currents for CSs and ICs for the period under study in Figure 8. Both latitudinal and longitudinal components show rather strong dispersion. At the same time, the along-track estimate of zonal component of geostrophic current shows remarkably low variations relative to a median value close to zero. On the contrary, the reanalysis predicts rather strong currents in the zonal direction. Both patterns, one of reanalysis and along-track estimates do not contradict observations but the dominance of meridional currents (north-south direction) looks more realistic.

In fact, there is a problem of along-track estimates as long as tracks are close to parallels in high latitudes and, thus, capture meridional currents (cross-track variations of SSHA) better than the reanalysis that smoothes data more or less isotropically.

4.3. Wind waves. Wave period estimates by altimetry

The short time delay between consecutive measurements in HLC is an essential gain for wind wave studies. In some cases it allows one to capture periods and directions of wave field that is, generally, unavailable from altimetry data using along-track records.

The reanalysis WAVERYS on a regular $1/5^\circ$ grid with a 3 hour time step of the Copernicus Marine Service has been used for demonstration features of the HLC data subset for the same time interval 17 October, 2016 – 27 October, 2016. The altimetry data are assimilated by MFWAM (Meteo-France WAve Model) taking into account oceanic currents from the GLORYS12 physical ocean reanalysis.

Preprints (www.preprints.org) | NOT PEER-REVIEWED | Posted: 8 January 2021 doi:10.20944/preprints202101.0137.v1

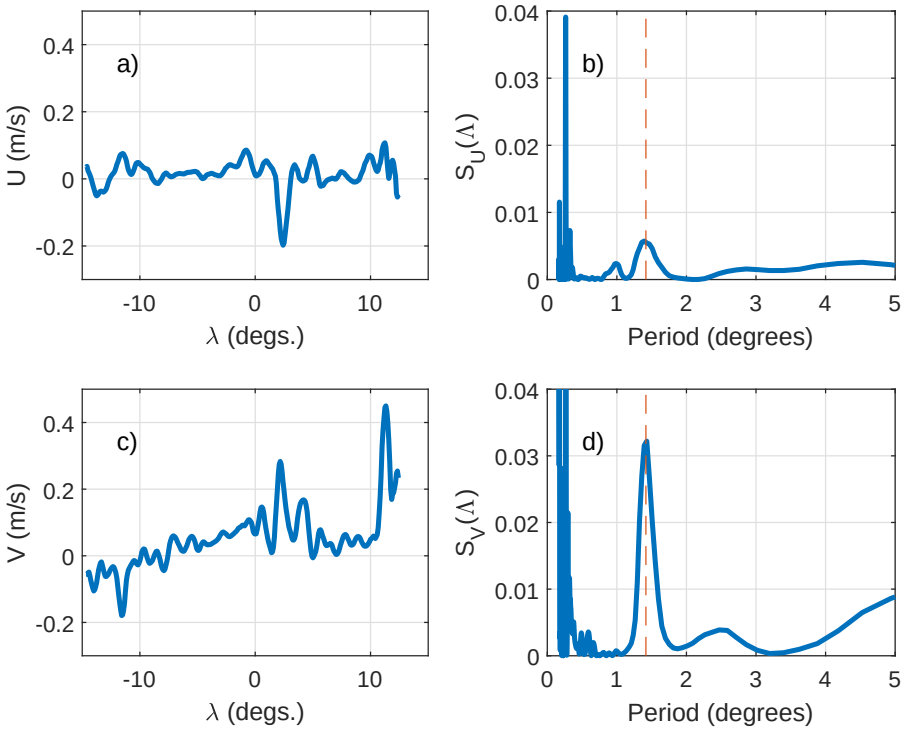

Figure 6. Transection along latitude 66°N on 17 October 2016. *a,c* – the current velocity components; *b,d* – spatial spectral densities of the current components vs spatial period (degrees).

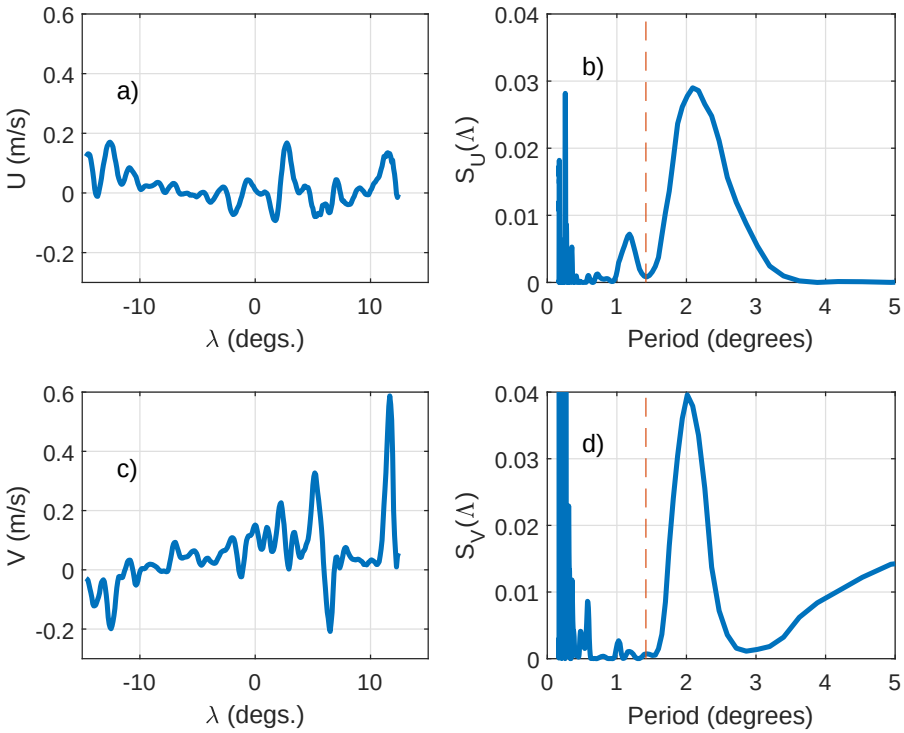

Figure 7. Same as in Figure 6 at transection along 66.5°N.

Preprints (www.preprints.org) | NOT PEER-REVIEWED | Posted: 8 January 2021 doi:10.20944/preprints202101.0137.v1

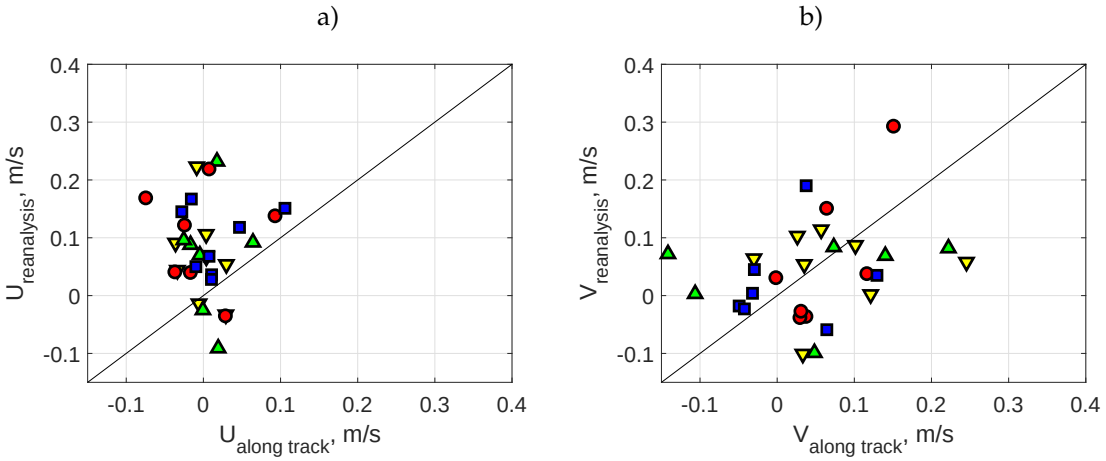

Figure 8. Scatterplot of current velocity components of the reanalysis vs along-track estimates of geostrophic currents. *a* – zonal; *b* – meridional components.

As expected, the wave heights measured by altimeters agree perfectly well with the reanalysis (not shown here). An essential result is good agreement of two consecutive measurements in the crossovers as illustrated by Figure 9*a*. Both ICs (triangles) with a delay of about 1 hour and SCs (circles and squares) with 2 hour delay show dispersion of about 30 cm that is close to the declared accuracy of wave height measurements by altimeters and ocean buoys [68].

Wave periods cannot be measured by altimeters directly but can be recovered within different approaches. The most used empirical parametrical models [e.g. 69–71] that postulates dependence of wave period on significant wave height H_s and the normalized radar cross-section (NRCS) σ_0 are able to provide the accuracy better than 1 s [71]. At the same time, validity of these models can be questionable for high latitudes where buoy measurements are absent and, thus, the models are not properly substantiated. Additionally, these parameterizations are mission dependent: every mission requires its own set of empirical coefficients.

Alternative models of wave periods [e.g. 20,72] rely upon physical links of wave parameters and, in this way, are less dependent on features of particular altimeter and particular sea state environment. Figure 9*b* shows quite good correspondence of the physical model (2,3) and the WAVERYS reanalysis for the spectral moments $(0,2)$, wave period

$$T_{m02} = 2\pi \left(\frac{\int\int \omega^2 E(\omega,\theta) d\omega d\theta}{\int\int E(\omega,\theta) d\omega d\theta} \right)^{-1/2}. \quad (6)$$

High deviation of the model from the reanalysis quantities occurs at relatively short periods less than 4 s (wavelength less than approximately 25 meters) where the model validity is questionable. In Figure 9*b* both track records in the crossovers are used to retrieve the "full" period in accordance with the scheme of Figure 4*b*. This "full" period does not differ significantly from its approximate counterpart when the full gradient $|\nabla H_s|$ is replaced by the along-track derivative of one of altimeters. We present the ascending track calculations in Figure 9*c* with less than 15% of the period overestimate.

Comparison of the physical model of Badulin [20] with its empirical counterpart of Gommenginger *et al.* [69] in Figure 9*d* discovers a remarkable similarity of two alternatives for the wave period from altimetry data. The excess of the period of Gommenginger *et al.* [69] over its counterpart of Badulin [20] is essentially higher than one fixed for a one-year period at ocean buoy sites [cf. Figure 2d in 21]. It can be explained by features of particular altimeters [Envisat in 21, and Jasons' in this study] . An alternative explanation: the effect of high latitudes where the empirical model [69] has never been tested.

The apparent correlation of the two period estimates demonstrates, in our opinion, a good potential of the parametric models regardless their quantitative fail. The pronounced linear correlation

Preprints (www.preprints.org) | NOT PEER-REVIEWED | Posted: 8 January 2021 doi:10.20944/preprints202101.0137.v1

of two models in Figure 9*d* signifies correspondence of the parametric representation to the inherent physical feature of sel-similarity of evolution of wind-driven waves.

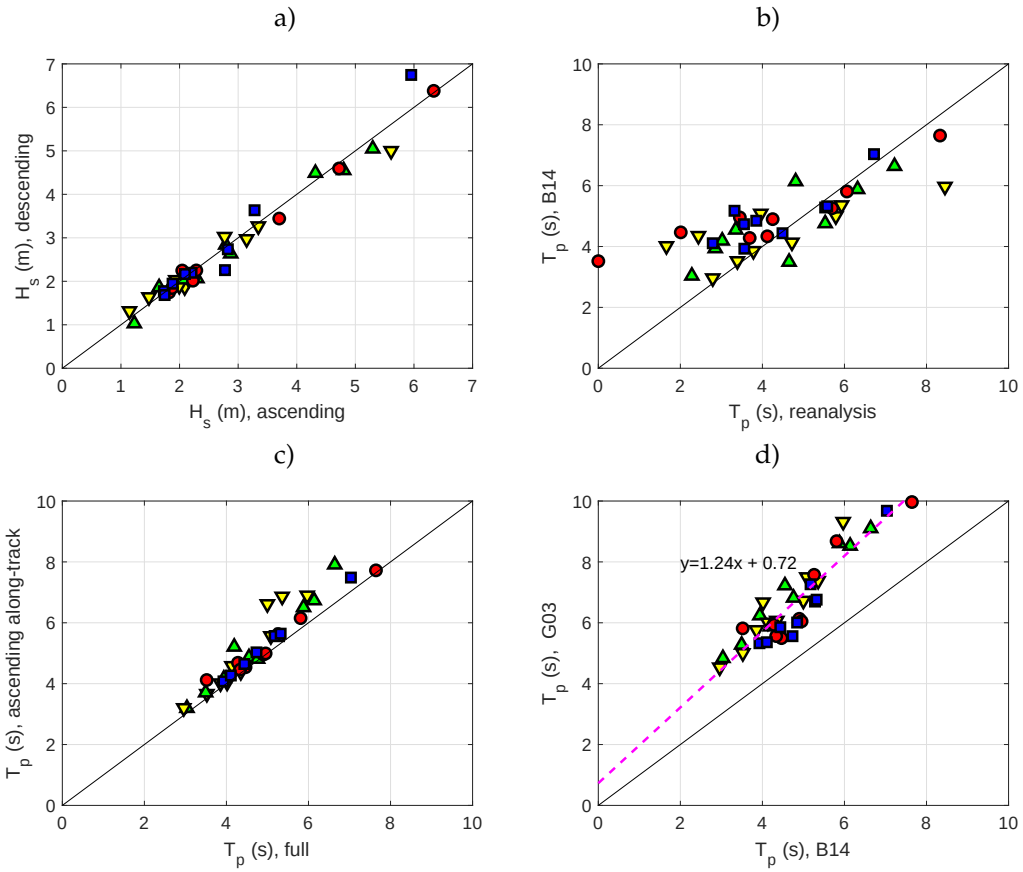

Figure 9. Scatterplots of wave parameters in HLCs. a) – significant wave heights; b) – wave periods of the model of Badulin [20] vs reanalysis; c) – single-track vs "full" periods of Badulin [20]; d) – periods with the model of Gommenginger *et al.* [69] vs Badulin [20].

5. Discussion and Conclusions

In the present paper we have proposed new essential add-on of satellite altimetry related to the peculiarities of the orbits of the Topex/Poseidon and Jasons (Jason-1, Jason-2, Jason-3) satellite missions which was not mentioned before in the scientific publications. The first one is related with the use of the "self-crossover" (SC) points that occur near the latitude of the Jason's orbits turn just below the Polar Circles where the satellite intersects its own orbit with one orbit period of 112 min. The second one is related to the "inter-crossover" points (IC) that occurs as intersection of tracks of interleaved orbits of two subsequent altimetry satellites with the time lag of about 1 hour (approximately one half of the orbit period).

One can summarize the useful features of the two types of crossovers in the following list:

1. Measurements at these crossovers are carried out by the same (in case of self-crossovers) or similar (in case of inter-crossovers) radar altimeters with the subsequent use of compatible processing and retracking procedures;
2. Points of both types of crossovers are the same within the accuracy of the altimeters' tracks. It permits to organize repetitive monitoring of currents, water exchange, wind and wave characteristics in these points with periods of full cycle for the SCs (about 10 days) and half-cycle (about 5 days) for ICs;

3. Short time lag of high latitude crossovers (HLC) less than 2 hours for SCs and about 1 hour for ICs (see Table 2) reduces the effect of variability of sea environment (sea state) even for such short-scale phenomenon as wind-driven waves;
4. Angles between tracks in the intersection points are large enough (about 30° for SCs and 15° for ICs) to get full vector of geostrophic current velocity and wave direction from along-track records. In the conventional satellite altimetry estimates of current velocity is usually based on interpolated fields of sea surface height anomaly that is associated with essential smoothing of instantaneous fields in time and space. The latter can essentially corrupt the resulting current field;
5. The number of these crossovers in the important ice-free Sub-Polar areas of the World Ocean is large enough to conduct permanent monitoring of key oceanographic parameters for ocean dynamics, marine meteorology and climate research;
6. In many regions, the latitudinal spatial distribution of these crossovers allows calculation of anomalies of water exchange between the most important sub-basins in the Sub-Arctic seas. It is interesting to apply this methodology to the Southern Ocean where these crossovers do not cross the Antarctic Circumpolar Current (ACC), its branches and fronts because the chain of these crossovers goes along the ACC and all the crossovers are located between the ACC and the coast of Antarctica.

The Norwegian Sea case study shows important advantages in the application of new technology for ocean dynamics, sea state and climate studies which was unattainable for conventional satellite altimetry. Our preliminary results showed a very good correspondence of the altimetry and reanalysis derived values of wind and wave characteristics measured in the Norwegian Sea. We encourage the altimetry community to pay attention to these new advantages of satellite altimetry and propose collaboration in studies of currents, water exchange, wind and wave characteristics in the Sub-Arctic seas and the Southern Ocean.

Author Contributions: Conceptualization, S.B. and V.G.; methodology, S.B, A.K., V.G., S.L. ; formal analysis, P.Sh., S.L.; data curation, P.Sh., V.Sh.; writing–original draft preparation S.B., A.K., V.G.; writing–review and editing V.G., V.Sh., S.L.; visualization, V.Sh., P.Sh.. All authors have read and agreed to the published version of the manuscript.

Funding: Sections 1,2 and 4 were done within the Russian Foundation of Basic Research project No 19-05-00147 (S.B., V.G., P. Sh., V.Sh.). A.K. (sect.3) was supported in the framework of the P.P. Shirshov Institute of Oceanology RAS state assignment No 0128-2021-0002. The case study was done in the framework of the Russian Foundation of Basic Research project No 18-05-80065.

Conflicts of Interest: "The authors declare no conflict of interest."

Abbreviations

The following abbreviations are used in this manuscript:

SC	self-crossover(s)
IC	inter-crossover(s)
STD	Standard deviation
HLC	sub-arctic crossovers
SSHA	sea surface height anomaly
PF	Polar Front
ACC	Antarctic Circumpolar Current
SB	the Southern Boundary
ASF	Antarctic Slope Front

References

[1] Wunsch, C.; Gaposchkin, E.M. On using satellite altimetry to determine the general circulation of the oceans with application to geoid improvement. *Rev. of Geophys.* **1980**, *18*, 725–745. doi:10.1029/RG018i004p00725.

[2] Wunsch, C.; Stammer, D. Satellite altimetry, the marine geoid, and the oceanic general circulation. *Annual Review of Earth and Planetary Sciences* **1998**, *26*, 219–253. doi:10.1146/annurev.earth.26.1.219.

[3] Fu, L.; Cazenave, A. *Satellite Altimetry and the Earth Sciences: A Handbook of Techniques and Applications*; Vol. 69, *International Geophysics Series*, Academic Press, 2001.

[4] Lebedev, S.; Kostianoy, A. *Satellite Altimetry of the Caspian Sea*; Sea: Moscow, 2005. 366 pp. (in Russian).

[5] Vignudelli, S.; Kostianoy, A.G.; Cipollini, P.; Benveniste, J., Eds. *Coastal Altimetry*; Springer-Verlag: Berlin, Heidelberg, 2011. doi:10.1007/978-3-642-12796-0.

[6] Lebedev, S.A. Satellite altimetry in the Earth Sciences. *Sovremennye problemy distantsionnogo zondirovaniya Zemli iz kosmosa* **2013**, *10*, 33–49. (in Russian).

[7] Frappart, F.; Andersen, O.; Lebedev, S.; Ramillien, G., Eds. *Satellite Altimetry for Earth Sciences*; MDPI: Basel. Beijing. Wuhan. Barcelona. Belgrade, 2019. 484 pp., doi:10.3390/books978-3-03897-681-3.

[8] Rosmorduc, V.; Srinivasan, M.; Richardson, A.; Cipollini, P. The first 25 years of altimetry outreach. *Adv. Space Res.* **2020**. doi:10.1016/j.asr.2020.08.026.

[9] International Altimetry Team Altimetry for the future: Interdisciplinary recommendations following the "25 Years of Progress in Radar Altimetry" Anniversary. *Adv. Space Res.* **2020**.

[10] Munk, W. Lecture 1:40–2:00 pm, Thursday, April 18. Southwest Regional Meeting April 18-19, 2002 Los Angeles, CA. The U.S. Commission on Ocean Policy, 2002.

[11] Stammer, D.; Cazenave, A., Eds. *Satellite altimetry over oceans and land surfaces*; CRC Press, 2017. 643 pp., doi:10.1201/9781315151779.

[12] Ablain, M.; Philipps, S.; Picot, N.; Bronner, E. Jason-2 global statistical assessment and cross-calibration with Jason-1. *Marine Geodesy* **2010**, *33*, 162–185. doi:10.1080/01490419.2010.487805.

[13] Gaspar, P.; Ogor, F.; Traon, P.Y.L.; Zanife, O.Z. Estimating the sea state bias of the TOPEX and POSEIDON altimeters from crossover differences. *J. Geophys. Res.* **1994**, *99*, 24,981–24, 994.

[14] Gommenginger, C.; Srokosz, M.; Bellingham, C.; Snaith, H.; Pires, N.; Fernandes, M.J.; Tran, N.; Vandemark, D.; Moreau, T.; Labroue, S.; Scharroo, R. Sea State Bias: 25 Years on. 25 years of progress in radar altimetry; 2018.

[15] Badulin, S.; Grigorieva, V.; Shabanov, P.; Sharmar, V.; Karpov, I. Sea state bias in altimetry measurements within the theory of similarity for wind-driven seas. *Advances in Space Research* **2019**. doi:10.1016/j.asr.2019.11.040.

[16] Abdalla, S. Ku-band radar altimeter surface wind speed algorithm. Proc. of the Envisat Symposium 2007, Montreux, Switzerland, 23-27 April 2007, 2007.

[17] Lebedev, S.A. Technique for processing satellite altimetry data for the waters of the White, Barents and Kara seas. *Modern problems of remote sensing of the Earth from space* **2016**, *13*, 203–223.

[18] Lebedev, S.; Kostianoy, A. Interannual variability of water exchange anomalies between the Northern, Middle and Southern Caspian based on satellite altimetry data. *Ecologica Montenegrina* **2019**, *25*, 106–115.

[19] Lebedev, S.; Kostianoy, A. Investigation of seasonal and interannual variability of water exchange through the Middle Caspian based on satellite altimetry. *Sovremennye problemy distantsionnogo zondirovaniya Zemli iz kosmosa* **2020**, *17*.

[20] Badulin, S.I. A physical model of sea wave period from altimeter data. *J. Geophys. Res. Oceans* **2014**, *119*, 856–869. doi:10.1002/2013JC009336.

[21] Badulin, S.; Grigorieva, V.; Gavrikov, A.; Geogjaev, V.; Krinitskiy, M.; Markina, M. Wave steepness from satellite altimetry for wave dynamics and climate studies. *Russ. J. Earth. Sci.* **2018**, *18*, ES5005. doi:10.2205/2018ES000638.

[22] Schlesinger, M.; N., R. An Oscillation in the global climate system of period 65-70 years. *Nature* **1994**, *367*, 723–726. doi:10.1038/367723a0.

[23] Kushnir, Y. Interdecadal variations in North Atlantic sea surface temperature and Associated Atmospheric Conditions. *Journal of Climate* **1994**, *7*, 141–157. doi:10.1175/1520-0442(1994)007<0141:IVINAS>2.0.CO;2.

[24] Delworth, T.L.; Mann, M.E. Observed and simulated multidecadal variability in the Northern Hemisphere. *Climate Dynamics* **2020**, *16*, 661–676. doi:10.1007/s003820000075.

[25] Lappo, S.S.; Gulev, S.K.; Dobrolyubov, S.A. In *Actual problems of oceanology*; Nauka: Moscow, 2003; chapter The North Atlantic and its impact on the climate of Europe, pp. 8–59.

[26] Byshev, V.I. *Synoptic and Large-Scale Variability of the Ocean and Atmosphere*; Nauka, Moscow, 2003. 344 pp. (in Russian).

[27] Sutton, R.T.; Hodson, D.L.R. Atlantic ocean forcing of North American and European summer climate. *Science* **2005**, *309*, 115–8. doi:10.1126/science.1109496.

[28] Sutton, R.T.; Dong, B. Atlantic Ocean influence on a shift in European climate in the 1990s. *Nature Geoscience* **2012**, *5*, 788–792. doi:10.1038/ngeo1595.

[29] Rodionov, V.B.; Kostianoy, A.G. *Oceanic Fronts of the North-European Basin Seas*; GEOS: Moscow, 1998. 293 pp. (in Russian).

[30] Kostianoy, A.G.; Nihoul, J.C.J.; Rodionov, V.B. *Physical Oceanography of Frontal Zones in the Subarctic Seas*; Vol. 71, *Elsevier Oceanography Series*, Elsevier, 2004. 316 pp.

[31] Davidan, I.N.; Lopatukhin, L.I. *Towards the storms*; Leningrad, Hydrometeoizdat, 1982. 136 pp, (in Russian).

[32] Reistad, M.; Breivik, O.; Haakenstad, H.; Aarnes, O.J.; Furevik, B.R.; Bidlot, J. A high-resolution hindcast of wind and waves for the North Sea, the Norwegian Sea, and the Barents Sea. *J. Geophys. Res.* **2011**, *116*, C05019. doi:10.1029/2010JC006402.

[33] Semedo, A.; Vettor, R.; Breivik, O.; Sterl, A.; Reistad, M.; Lima, D.C.A. The wind sea and swell waves climate in the Nordic seas. *Ocean Dynamics* **2014**, *65*. doi:10.1007/s10236-014-0788-4.

[34] Jonsson, S.; Valdimarsson, H. A new path for the Denmark Strait overflow water from the Iceland Sea to Denmark Strait. *Geophys. Res. Lett.* **2004**, *31*, L03305. doi:10.1029/2003GL019214.

[35] Pickart, R.S.; Spall, M.A.; Torres, D.J.; Vage, K.; Valdimarsson, H.; Nobre, C.; Moore, G.W.K.; Jonsson, S.; Mastropole, D. The North Icelandic Jet and its relationship to the North Icelandic Irminger Current. *J. Mar. Res.* **2017**, *75*, 605–639. doi:10.1357/002224017822109505.

[36] Semper, S.; Vage, K.; Pickart, R.; Valdimarsson, H.; Torres, D.J.; Jonsson, S. The emergence of the North Icelandic Jet and its evolution from Northeast Iceland to Denmark Strait. *J. Phys. Oceanogr.* **2019**, *49*, 2499–2521.

[37] Cappelen, J.; Jorgensen, B.V.; Laursen, E.V.; Stannius, L.S.; Thomsen, R.S. *The observed climate of Greenland, 1958-99 – with climatological standard normals 1961-90*; Danish Meteorological Institute, Copenhagen, 2001. 152 pp.

[38] Silber, G.K.; Adams, J.D. Vessel operations in the Arctic, 2015-2017. *Frontiers in Marince Science* **2019**, *6*. doi:10.3389/fmars.2019.00573.

[39] Christensen, T.; Lasserre, F.; Dawson, J.; Guy, E.; Pelletier, J.F., Adaptation Actions for a Changing Arctic: Perspectives from the Baffin Bay/Davis Strait Region; Oslo: Arctic Monitoring and Assessment Programme (AMAP), 2018; chapter Shipping, pp. 243–259.

[40] Filatov, N.; Pozdnyakov, D.; Johannessen, O.M.; Pettersson, L.H.; Bobylev, L.P. *White Sea. Its Marine Environment and Ecosystem Dynamics Influenced by Global Change*; Springer-Praxis, 2005. 463 pp.

[41] Lisitzin, A.P.; Shevchenko, V.P.; Gordeev, V.V.; Kravchishina, M.D.; Pantyulin, A.N.; Kosobokova, K., Eds. *The White Sea System*; Vol.2 Water column and the atmosphere, cryosphere, river runoff and biosphere interacting with it, Nauchny Mir: Moscow, 2012. 782 pp. (in Russian).

[42] Lisitzin, A.P.; Gordeev, V.V., Eds. *Biogeochemistry of the Atmosphere, Ice and Water of the White Sea. The White Sea Environment. Part I*; Springer Nature Switzerland AG, Cham: Switzerland, 2018. 327 pp.

[43] Lisitzin, A.P.; Demina, L.L., Eds. *Sedimentation Processes in the White Sea. The White Sea Environment. Part II*; Springer Nature Switzerland AG, Cham: Switzerland, 2018. 311 pp., doi:10.1007/978-3-030-05111-2.

[44] Lopatukhin, L.I.; Bukhanovsky, A.V.; Chernysheva, E.S. *Reference Data on Wind-Wave Regime in the Bering and White Seas*; Russian Maritime Register of Shipping: St.-Petersburg, 2010. 566 pp. (in Russian).

[45] Badulin, S.I.; Grigorieva, V.G.; Shabanov, P.A.; Sharmar, V.D.; Karpov, I.; Lebedev, S.A.; Kostianoy, A. Case study of wind-driven waves in the White Sea during the tandem phase of Jason-2 and Jason-3 missions. Coastal Altimetry Workshop 12, 4-7 February 2020. Frascati, Italy, 2020.

[46] Badulin, S.I.; Grigorieva, V.G.; Shabanov, P.A.; Sharmar, V.D.; Lebedev, S.A.; Kostianoy, A.G. Altimeter crossovers for monitoring waves and currents in the White Sea. Waves in Shallow water Environment. Bergen, Norway, 10-14 May 2020, 2020.

[47] Lebedev, S.A.; Zilberstein, O.I.; Popov, S.K.; Tikhonova, O.V. In *Satellite Altimetry for Geodesy, Geophysics and Oceanography*; Hwang, C.; Shum, C.K.; Li, J.C., Eds.; Heidelberg: Springer Verlag: Berlin, 2004; Vol. 126, *IAG Symposia*, chapter Analysis of temporal sea level variation in the Barents and the White Seas from altimetry, tide gauges and hydrodynamic simulation, pp. 243–249. doi:10.1007/978-3-642-18861-9_30.

[48] Lebedev, S.A.; Kostianoy, A.G.; Ginzburg, A.I.; Medvedev, D.P.; Sheremet, N.A.; Shauro, S.N. The ALTICORE Project: The Barents and White seas. Int. Conf. Electronic Geophysical Year: State of the Art and Results; , 2009; p. 49. doi:10.2205/2009-REGYconf.

[49] Lebedev, S.A.; Kostianoy, A.G.; Ginzburg, A.I.; Medvedev, D.P.; Sheremet, N.A.; Shauro, S.N. In *Satellite altimetry applications in the Barents and White seas*; Vignudelli, S.; A. G. Kostianoy, P. Cipollini, J.B., Eds.; Springer-Verlag: Berlin, Heidelberg, 2011; chapter Coastal Altimetry, pp. 389–415. doi:10.1007/978-3-642-12796-0_15.

[50] Lebedev, S.A.; Bogoutdinov, S.R.; Nekhoroshev, S.A.; Kravchenko, P.N. Identification of the Baltic and White Seas ice cover based on satellite altimetry and radiometry. IEEE/OES Baltic International Symposium (BALTIC). IEEE, 2018, pp. 1–4. doi:10.1109/BALTIC.2018.8634847.

[51] Lebedev, S.A.; Kostianoy, A.G. Seasonal and interannual sea level and ice fraction variability in the Barents and White seas based on remote sensing data. 2-6 December 2008, Guangzhou, China. PORSEC, 2008, p. 34.

[52] Coachman, L.; Aagaard, K.; Tripp, R.B. *Bering Strait: The Regional Physical Oceanography*; Seattle, University of Washington Press, 1975. 172 pp.

[53] Walsh, J.J.; McRoy, C.P.; Coachman, L.K.; Goering, J.J.; Nihoul, J.C.J.; Whitledge, T.E.; Blackburn, T.; Parker, P.L.; Wirick, C.D.; Shuert, P.G.; Grebmeier, J.M.; Springer, A.M.; Tripp, R.D.; Hansell, D.; Djenidi, S.; Deleersnijder, E.; Henriksen, K.; Lund, B.A.; Andersen, P.; Muller-Karger, F.E.; Dean, K. Carbon and nitrogen cycling within the Bering/Chukchi Sea: source regions for organic matter affecting AOU demands of the Arctic Ocean. *Progr. Ocean.* **1989**, *22*, 277–359.

[54] Nihoul, J.C.J., Marine Interfaces Ecohydrodynamics; Elsevier: Amsterdam, 1986; chapter Aspects of the Northern Bering Sea Ecohydrodynamics, pp. 385–399.

[55] Nihoul, J.C.J. *Application of Mathematical Modelling to the Marine Environment*; E. Riga Publ.: Liege. 69 pp.

[56] Nihoul, J.C.J.; Adam, P.; Brasseur, P.; Deleersnijder, E.; Djenidi, S.; Haus, J. Three-dimensional general circulation model of the northern Bering Sea's summer ecohydrodynamics. *Continental Shelf Research* **1993**, *13*, 509–542.

[57] Nihoul, J.C.J.; Adam, P.; Brasseur, P., Data assimilation. Tools for modelling the ocean in a global change perspective; NATO ASI Series 19, Springer-Verlag, 1994; chapter Mathematical visualisation of the Northern Bering Sea's summer ecohydrodynamics, pp. 107–134.

[58] Sokolov, S.; Rintoul, S.R. Structure of Southern Ocean fronts at 140°E. *J. Mar. Sys.* **2002**, *37*, 151–184.

[59] Sokolov, S.; Rintoul, S.R. Circumpolar structure and distribution of the Antarctic Circumpolar Current fronts: 2. Variability and relationship to sea surface height. *J. Geophys. Res.* **2009**, *114*, C11019. doi:10.1029/2008JC005248.

[60] Ginzburg, A.I.; Kostianoy, A.G.; Frankignoulle, M.; Delille. Investigations of fronts in the southern part of the Indian Ocean by satellite temperature data. *Issledovanie Zemli iz kosmosa* **2002**, *5*, 39–49. in Russian.

[61] Kostianoy, A.G.; Ginzburg, A.I.; Lebedev, S.A.; Frankignoulle, M.; Delille, B. Fronts and mesoscale variability in the Southern Indian Ocean as inferred from altimetric data of TOPEX/POSEIDON and ERS-2. *Oceanology* **2003**, *43*, 632–642.

[62] Koshlyakov, M.N.; Tarakanov, R. Y. Savchenko, D.S. Energy interaction of the jets and eddies of Antarctic Circumpolar Current in the near-surface layer of the Southern Ocean. *Journal of Oceanological Research* **2019**, *47*, 39–57. in Russian, doi:10.1134/S0001437019030093.

[63] Badulin, S.I.; Babanin, A.V.; Resio, D.; Zakharov, V. Weakly turbulent laws of wind-wave growth. *J. Fluid Mech.* **2007**, *591*, 339–378.

[64] Gagnaire-Renou, E.; Benoit, M.; Badulin, S.I. On weakly turbulent scaling of wind sea in simulations of fetch-limited growth. *J. Fluid Mech.* **2011**, *669*, 178–213.

[65] Zavadsky, A.; Shemer, L. Water waves excited by near-impulsive wind forcing. *J. Fluid Mech.* **2017**, *828*, 459–495. doi:10.1017/jfm.2017.521.

[66] Shemer, L. On Evolution of young wind waves in time and space. *Atmosphere* **2019**, *10*, 1–54. doi:10.3390/atmos10090562.

[67] Shemer, L.; Singh, S.K.; Chernyshova, A. Spatial evolution of young wind waves: numerical modelling verified by experiments. *J. Fluid Mech.* **2020**, *901*. doi:10.1017/jfm.2020.549.

[68] Dumont, J.P.; Rosmorduc, V.; Picot, N.; Bronner, E.; Desai, S.; Bonekamp, H.; Figa, J.; Lillibridge, J.; Scharroo, R. *OSTM/Jason-2 Products Handbook*. CNES: SALP-MU-M-OP-15815-CN, EUMETSAT:

EUM/OPS-JAS/MAN/08/0041, JPL: OSTM-29-1237, NOAA/NESDIS: Polar Series/OSTM J400, issue: 1 rev 8 ed., 2011.

[69] Gommenginger, C.P.; Srokosz, M.A.; Challenor, P.G.; Cotton, P.D. Measuring ocean wave period with satellite altimeters: A simple empirical model. *Geophys. Res. Lett.* **2003**, *30*, 2150. doi:10.1029/2003GL017743.

[70] Quilfen, Y.; Chapron, B.; Serre, M. Calibration/validation of an altimeter wave period model and application to TOPEX/Poseidon and Jason-1 altimeters. *Marine Geodesy* **2004**, *27*, 535–549.

[71] Mackay, E.B.L.; Retzler, C.H.; Challenor, P.G.; Gommenginger, C.P. A parametric model for ocean wave period from Ku-band altimeter data. *J. Geophys. Res.* **2008**, *113*. doi:10.1029/2007JC004438.

[72] Hwang, P.A.; Teague, W.J.; Jacobs, G.A.; Wang, D.W. A statistical comparison of wind speed, wave height and wave period derived from satellite altimeters and ocean buoys in the Gulf of Mexico region. *J. Geophys. Res.* **1998**, *103*, 10451–10468.